Microstructure of compositionally-graded $(Ba_{1-x}Sr_x)TiO_3$ thin films epitaxially grown on $La_{0.5}Sr_{0.5}CoO_3$-covered (100) $LaAlO_3$ substrates by pulsed laser deposition

Xinhua Zhu[a)]
National Laboratory of Solid State Microstructures, Department of Physics, Nanjing University, Nanjing 210093, People's Republic of China and Max-Planck-Institut für Mikrostrukturphysik, Weinberg 2, D-06120 Halle, Germany

Helen Lai-Wah Chan, Chung-Loong Choy, and Kin-Hung Wong
Department of Applied Physics and Materials Research Center, The Hong Kong Polytechnic University, Hung Hom, Hong Kong, People's Republic of China

Dietrich Hesse
Max-Planck-Institut für Mikrostrukturphysik, Weinberg 2, D-06120 Halle, Germany

(Received 3 December 2004; accepted 7 February 2005; published online 14 April 2005)

Compositionally-graded $(Ba_{1-x}Sr_x)TiO_3$ (BST) epitaxial thin films (with x decreasing from 0.25 to 0.0) were deposited by pulsed laser deposition on (100)$LaAlO_3$ (LAO) single-crystal substrates covered with a conductive $La_{0.5}Sr_{0.5}CoO_3$ (LSCO) layer as a bottom electrode. X-ray and electron diffraction patterns demonstrate that the entire graded film has a single-crystal cubic structure. The epitaxial relationship between BST, LSCO, and LAO can be described as $(100)_{BST}\|(100)_{LSCO}\|(100)_{LAO}$; $[001]_{BST}\|[001]_{LSCO}\|[001]_{LAO}$. Cross-sectional transmission electron microscopy (TEM) images reveal that both the BST films and the LSCO bottom electrodes have sharp interfaces and overall uniform thickness across the entire specimen, and that they grow with a columnar structure. Planar TEM images show that the graded films exhibit granular and/or polyhedral morphologies with an average grain size of 50 nm. High-resolution TEM images reveal aligned rectangular-shaped voids in the graded BST film, with length size of 12–17 nm, and width of 5–8 nm along the ⟨001⟩ direction in the (100) plane. © *2005 American Institute of Physics*. [DOI: 10.1063/1.1882766]

I. INTRODUCTION

Recently dielectric $(Ba_{1-x}Sr_x)TiO_3$ (BST) thin films have been considered to be important materials for tunable microwave devices (e.g., microwave tunable phase shifters, filters, oscillators, and antennas) due to their high dielectric constant, relatively low dielectric loss, and large electric field tunability.[1–9] These tunable devices are based on a large electric-field dependent dielectric constant, which results in a change in phase velocity in the device, allowing it to be tuned in real time for particular applications.[10] For optimum performance of these devices, it is important to grow BST thin films with high dielectric tunability ($\Delta\varepsilon_r/\varepsilon_r$, ε_r is the dielectric constant), low microwave losses (or high quality factor Q), and low temperature dependence of the dielectric constants in the operational frequency range of the device and in the corresponding temperature range.[11,12] Although much progress has been made in recent years both in the deposition of high quality BST thin films and in the performance of BST thin film-based microwave devices,[13–17] to date, the actual use of BST thin films for microwave applications is still hampered by high microwave losses and the large temperature dependence of the dielectric constants. Furthermore, there is still concern about the reliability of microwave devices over the operating frequency and temperature ranges. BST films have a high dielectric constant in the paraelectric phase above the Curie temperature (which depends upon the composition, x). However, they are not suitable for practical applications to microwave devices in the device operating temperature range due to the temperature dependence of the dielectric constants in the paraelectric phase following the Curie–Weiss law.[18,19] Thus, it is necessary to grow BST thin films with a low temperature dependence of the dielectric constant for actual microwave applications, which can be approached by using compositionally-graded structures.[20] Since high-angle grain boundaries increase the dielectric loss and consequently limit the performance of the device, for microwave applications, grain-oriented and/or epitaxial films are highly required because of their high dielectric constant and large tunability.[9] Recently epitaxial BST films with compositionally-graded structure grown by pulsed laser deposition have been reported, and the dielectric properties and microwave performance of tunable devices based on such graded BST thin films have been characterized.[21–26] However, their microstructure has not yet been studied in detail. In this work, we report on epitaxial growth and microstructure of compositionally-graded epitaxial BST films grown by pulsed-laser deposition on (100)$LaAlO_3$ single-crystal substrates covered with a conductive $La_{0.5}Sr_{0.5}CoO_3$ (LSCO) bottom electrode. The epi-

[a)]Electronic mail: xhzhu@mpi-halle.de. Present address: Condensed Matter Physics and Materials Science, School of Mathematics and Physics, Queen's University of Belfast, Belfast BT7 1NN, United Kingdom.

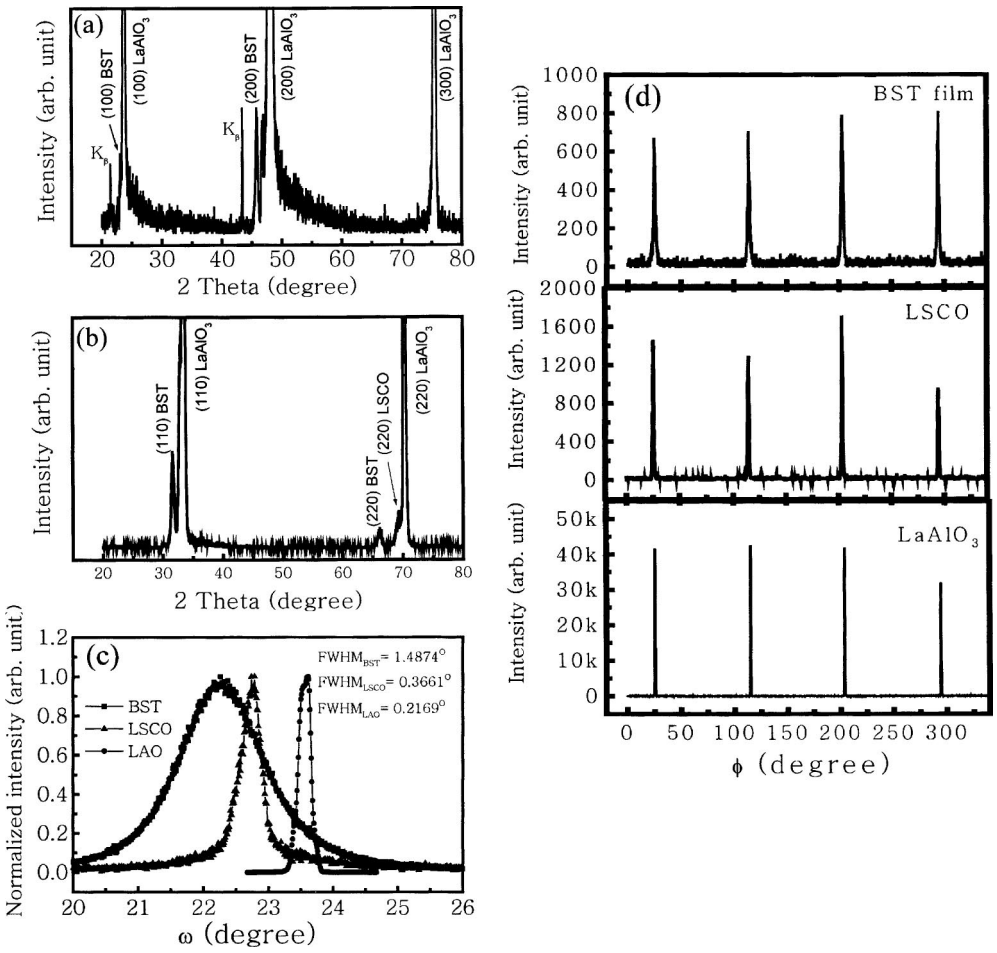

FIG. 1. Specular and off-specular x-ray diffraction scans of graded BST films deposited on the $(100)LaAlO_3$ substrate with LSCO as a bottom electrode: (a) specular θ–2θ scan, and (b) off-specular θ–2θ scan along the [110] direction of $LaAlO_3$. (c) shows the (200) rocking curves of BST, LSCO, and LAO, respectively, and (d) shows ϕ scans on the (220) reflections of BST, LSCO, and LAO, respectively.

taxial growth relationships between BST, LSCO, and the single crystal substrates are examined by x-ray diffraction and electron diffraction. The microstructure of epitaxially graded BST films was investigated by (high-resolution) transmission electron microscopy (TEM) from both plan-view and cross-sectional specimens.

II. EXPERIMENT

Compositionally-graded $(Ba_{1-x}Sr_x)TiO_3$ thin films (with x decreasing from 0.25 at the bottom to 0.0 at the top) were epitaxially grown on (100)LAO single-crystal substrates with a conductive LSCO layer as a bottom electrode. BST film growth was performed at 650 °C in an oxygen ambient pressure of 27 Pa by pulsed-laser deposition (PLD). Before deposition of the BST graded thin film, a LSCO bottom electrode was first deposited by PLD onto the (100)LAO substrate at 600 °C and an oxygen pressure of 20 Pa. The graded films were *in situ* deposited epitaxially on the top surface of the LSCO layer. The top layer of the graded BST film had the composition of $BaTiO_3$. Details of the deposi-

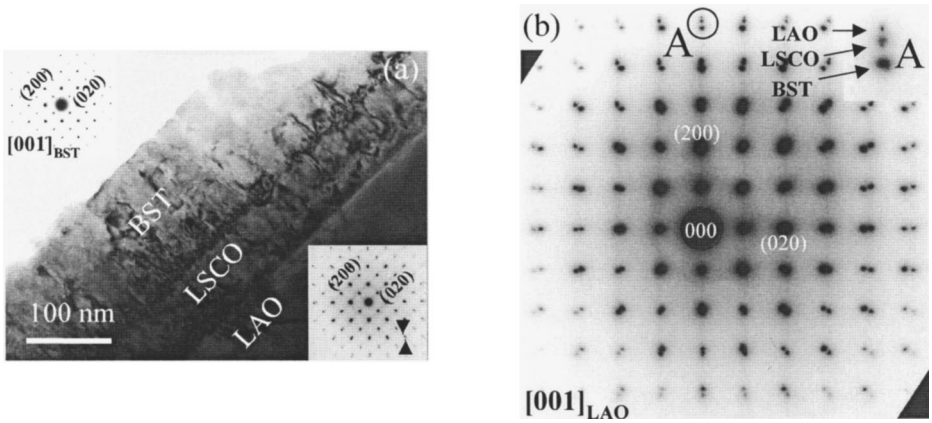

FIG. 2. (a) Bright-field cross-sectional TEM image of a graded BST film deposited on a $(100)LaAlO_3$ single crystal substrate, viewed along the $[001]_{LAO}$ direction. The two insets in (a) show the SAED patterns taken along the [001] direction from the graded BST film, and from the interface between LSCO (bottom electrode) and the substrate LAO, respectively. (b) A SAED pattern recorded using a selected area aperture covering the whole BST film, LSCO bottom electrode and, in addition, part of the substrate with the electron beam parallel to $[001]_{LAO}$.

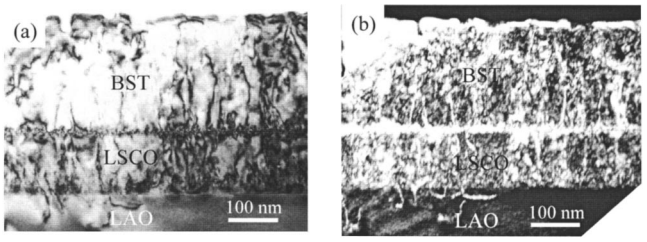

FIG. 3. Cross-sectional TEM images of a graded BST film viewed from the $[01\bar{1}]_{LAO}$ direction. (a) Bright-field image, and (b) dark-field image recorded using the almost coinciding (200) reflections of BST, LSCO, and LAO.

tion procedure were described elsewhere.[23] The thickness of the LSCO bottom electrode and the graded BST films were about 135 nm and 240 nm, respectively, measured by cross-sectional TEM. The compositional gradients were determined by Rutherfold backscattering spectroscopy (RBS, not shown here, cf. Ref. 21). The epitaxial growth and microstructure of the compositionally-graded BST films were characterized by x-ray diffraction patterns, rocking curves, and ϕ scans (XRD, Philips X'Pert X-ray diffractometer, Cu $K\alpha$ radiation at 30 kV), and (HR)TEM. Both cross-sectional and plan-view specimens were used for the microstructural investigations. Cross-sectional specimens were prepared by cutting the sample into slices along the $(001)_{LAO}$ and $(011)_{LAO}$ planes. Two slices were glued together face-to-face joining the film-covered surface. After the glue cured, disks with a diameter of 3 mm were obtained by cutting away redundant epoxy. These disks were then ground, dimpled, and polished, followed by Ar-ion milling in a Gatan Precision Ion Polishing System (PIPS, Model 691) at 4 keV with an incident angle of 6°. Plan-view samples were prepared by cutting disks with a diameter of 3 mm from the graded film using an ultrasonic cutter. These disks were ground, dimpled, and finally thinned to perforation by Gatan dual ion-milling (Model 600) from the substrate side. Electron diffraction patterns and TEM images were recorded in a Philips CM20T electron microscope operated at 200 kV, and high-resolution TEM (HRTEM) investigations were performed in a JEOL JEM-4010 high-resolution microscope operated at 400 kV.

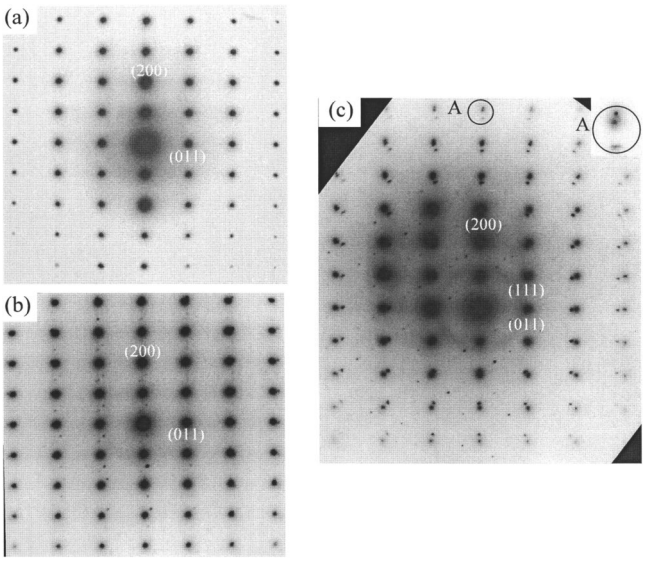

FIG. 4. SAED patterns taken from (a) BST layer, (b) the interface region between BST and LSCO, and (c) the entire layers along the $[0\bar{1}1]_{LAO}$ direction.

III. RESULTS AND DISCUSSION

Crystallographic indexing in this work is based on the following unit cell parameters: the nominal lattice parameters are $a_{LAO}=0.379$ nm; $a_{LSCO}=0.381$ nm; $a_{BaTiO_3}=0.3992$ nm; $c_{BaTiO_3}=0.4036$ nm; $a_{BST}=0.3977$ nm (BST, $x=0.23$); $c_{BST}=0.3988$ nm (BST, $x=0.23$) (for the latter two values, see the JCPDS card No. 44-0093). To characterize crystallinity and epitaxy of the compositionally-graded BST films, x-ray diffraction $\theta-2\theta$ scans, rocking curves, and ϕ scan studies were carried out. Figures 1(a) and 1(b) show specular and off-specular XRD scans. It is clearly observed in Fig. 1(a) that prominent BST (100) and (200) diffraction peaks appeared together with (h00) peaks of $LaAlO_3$. This indicates that the graded BST film is highly (100)-oriented with its surface parallel to that of the (100)LAO substrate. Similarly, the (110) plane of the graded BST film is also parallel to that of the LAO substrate, as shown in Fig. 1(b). Figure 1(c) shows the (200) ω-scan rocking curves of BST, LSCO, and LAO, respectively. The full width at half maximum (FWHM) of the BST (200) rocking curve was about 1.49°, which is relatively large indicating a certain level of mosaicity present in the graded BST film. This is confirmed by cross-sectional TEM images (see below). As shown in Fig. 1(b), the presence of BST (110) and (220) reflections oriented with respect to the {110} reflection of LAO displays the single crystal nature of the grown film and reveals the in-plane epitaxial relationship between the graded BST film and the LAO substrate: $(100)_{BST}\|(100)_{LAO}$ and $[001]_{BST}\|[001]_{LAO}$. Figure 1(d) shows the XRD 360° ϕ scan on the (220) reflections of BST, LSCO, and LAO, respectively. These reflections clearly demonstrate a good epitaxial growth of the graded BST film and the LSCO bottom electrode on the (100)LAO substrate. Both the BST film and the LSCO bottom electrode show a fourfold symmetry, indicating a cube-on-cube epitaxial growth.

To better understand the epitaxial growth of the graded film, TEM investigations were performed on two kinds of cross-sectional TEM specimens, which were prepared by cutting the sample into slices along $(001)_{LAO}$ and $(011)_{LAO}$ planes, respectively. A bright-field cross-sectional TEM image, viewed along the $[001]_{LAO}$ direction is shown in Fig. 2(a). It is observed that the graded BST film and the LSCO bottom electrode layer have sharp interfaces and overall uniform thickness over the entire specimen. However, some undulation can be seen along the surface of the graded BST film, thus indicating a 3D island growth. The thickness of the graded BST film was measured to be 240 nm, and that of the bottom LSCO electrode layer was 135 nm. Both LSCO and BST grow with a columnarlike structure along the $[100]_{LAO}$ direction, and the surface morphology of the graded BST film seems to involve some roughness in the order of 10 nm. The two insets in Fig. 2(a) are the selected area electron diffraction (SAED) patterns taken along the $[001]_{LAO}$ direction from the graded BST film and the interface between the

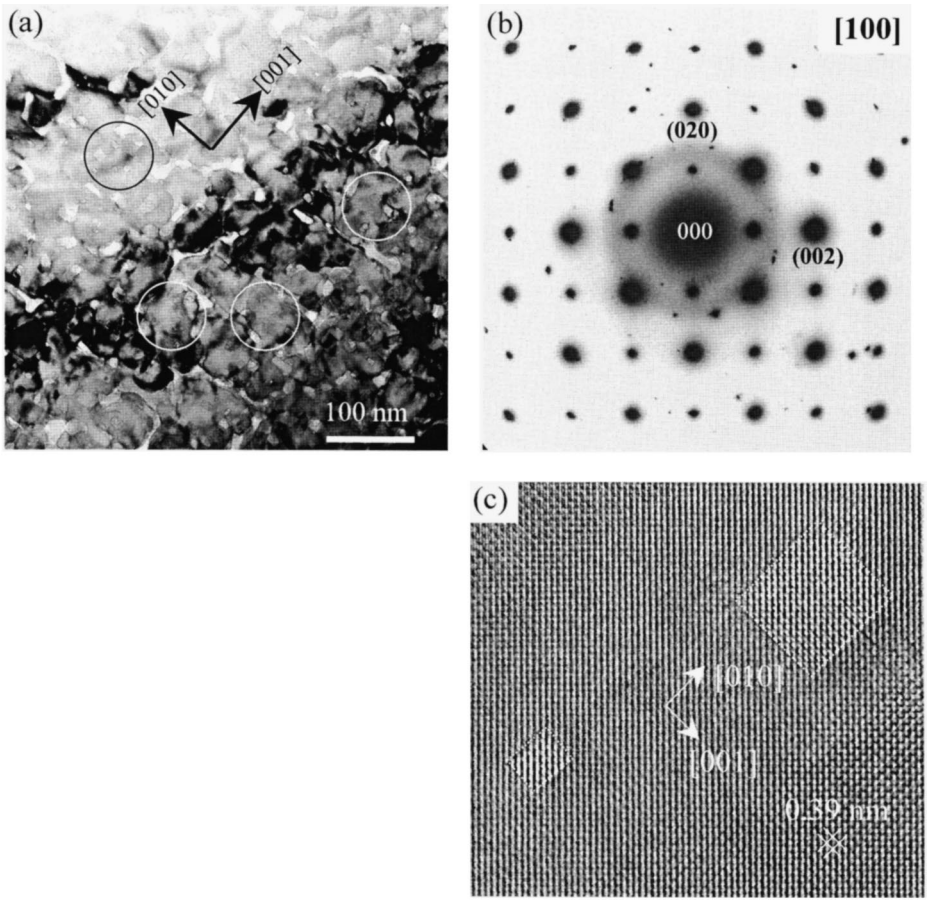

FIG. 5. (a) Bright-field TEM image taken from a planar sample, and (b) a SAED pattern taken from the same sample along the $[100]_{BST}$ direction. (c) High-resolution TEM image of fine aligned rectangular-shaped voids observed in a planar BST film.

LSCO bottom electrode and the substrate LAO, respectively. The sharp electron diffraction spots with no satellites or broadening indicate that the BST film has good epitaxial crystallinity. The good epitaxial growth of the LSCO bottom electrode on the LAO substrate is also confirmed: The corresponding diffraction pattern is a simple superposition of the LSCO bottom electrode and the LAO substrate. The differences in the lattice parameters in the (001) plane for LSCO and LAO can be clearly seen from the occurrence of the split of reflection spots along the horizontal and vertical directions, as indicated in the SAED pattern. Figure 2(b) is a SAED pattern recorded using a selected area aperture covering the whole BST film, LSCO bottom electrode and, in addition, part of the substrate with the electron beam parallel to the [001] axis of the substrate, which contains the crystallographic information for the film, LSCO and the LAO substrate. From the SAED pattern the reflection spots of the film, LSCO bottom electrode, and the substrate can be identified and particularly indexed using the notation of the perovskite pseudocubic basic cells. Furthermore, the triple-split of the reflection spots of BST, LSCO, and LAO along the horizontal and vertical directions in the (001) plane is clearly observed, which is due to the difference in the lattice parameters between BST, LSCO, and the LAO substrate. Taking the reflections and the bulk lattice parameter of the substrate LAO ($a_{LAO}=0.379$ nm) as a calibration standard, the lattice parameters for BST and LSCO layers in the (001) plane are calculated from the superposed electron diffraction patterns. The results show that a_{BST} calculated from the SAED pattern is about 2.0% larger than that determined from the XRD pattern, and that the one for LSCO is 2.3% larger than that from the XRD pattern. Considering the usual uncertainty (±5%) in SAED patterns this is a reasonable agreement. Based on the above SAED patterns the epitaxial orientation relationship between BST, LSCO, and the substrate LAO can be determined as $(100)_{BST}\|(100)_{LSCO}\|(100)_{LAO}$ and $[001]_{BST}\|[001]_{LSCO}\|[001]_{LAO}$, which agrees well with the XRD result. Bright- and dark-field cross-sectional TEM images of the graded BST film viewed from the $[01\bar{1}]_{LAO}$ direction are shown in Figs. 3(a) and 3(b), respectively. The dark-field image was recorded using the almost coinciding (200) reflections of BST, LSCO, and LAO. It is observed that the BST film and LSCO bottom electrode grow with a columnarlike structure along the [100] direction. The columnar texture of the graded BST film is most probably due to the presence of low-angle grain boundaries, resulting in a FWHM of the BST (200) ω-scan rocking curve as large as 1.49°. The SAED patterns taken from the BST layer, the interface between BST and LSCO, and the total layers with the electron beam parallel to the $[0\bar{1}1]_{LAO}$ direction, are shown in Figs. 4(a)–4(c), respectively. All the SAED patterns can be well indexed by using the notation of the perovskite pseudocubic basic cells. Again, the triple-split of the reflection spots of BST, LSCO, and LAO along the horizontal and vertical directions in the (011) plane is clearly observed, and the epitaxial growth relationship between BST,

LSCO, and the substrate LAO is confirmed. Some extra reflections are also visible in Figs. 4(b) and 4(c), which obviously result from a double diffraction effect.

The microstructure of the graded BST film was also studied by plan-view TEM that permits to investigate the microstructure over a large area. Figure 5 shows a bright-field TEM image taken from a planar sample [Fig. 5(a)] and the SAED pattern taken from the same sample along the $[100]_{BST}$ direction [Fig. 5(b)]. As shown in Fig. 5(a), the grains of the graded film exhibit granular and/or polyhedral morphologies with an average grain size of 50 nm. The diffraction pattern can be well indexed by using the perovskite cubic cells, indicating the lattice parameters *b* and *c* of the graded BST film are the same, as well as equal to the lattice parameter *a*. Thus, the graded BST film is of cubic structure. In addition, in Fig. 5(a) there are some aligned rectangular-shaped voids present in the graded BST film. Some of them are marked by circles. Their length varies from 12 to 17 nm, and the width is in the range of 5–8 nm. Their orientation relationship with the BST grain is revealed by the high-resolution TEM image, Fig. 5(c). Some extra diffraction spots with random distribution in Fig. 5(b) are observed, which possibly stem from residues of the bottom electrode in the thick area of the planar TEM specimen.

IV. CONCLUSIONS

Compositionally-graded $(Ba_{1-x}Sr_x)TiO_3$ thin films (with *x* decreasing from 0.25 to 0.0) were epitaxially grown by pulsed laser deposition on $(100)LaAlO_3$ (LAO) single-crystal substrates with a conductive $La_{0.5}Sr_{0.5}CoO_3$ (LSCO) layer as a bottom electrode. Their epitaxial growth and microstructure were investigated by x-ray diffraction, selected area electron diffraction, and (high-resolution) transmission electron microscopy. The results show that the as-grown films are cube-on-cube oriented with an orientation relationship of $(100)_{BST}\|(100)_{LSCO}\|(100)_{LAO}$; $[001]_{BST}\|[001]_{LSCO}\|[001]_{LAO}$. Cross-sectional TEM images reveal that both the BST film and the LSCO bottom electrode grow with a columnar structure, with sharp interfaces and overall uniform thickness across the entire specimen. Planar TEM images demonstrate that the BST grains have granular and/or polyhedral morphologies with an average grain size of 50 nm. Well-aligned rectangular-shaped voids with length size of 12–17 nm, and width of 5–8 nm were observed to be present in the BST films.

ACKNOWLEDGMENTS

This work is financially supported by the opening project of National Laboratory of Solid State Microstructures, Nanjing University, and by a grant for State Key Program for Basic Research of China. One of the authors (X.H. Zhu) acknowledges the financial support from the Alexander von Humboldt Foundation.

[1] J. Im, O. Auciello, P. K. Baumann, S. K. Streiffer, D. Y. Kaufman, and A. R. Krauss, Appl. Phys. Lett. **76**, 625 (2000).
[2] B. A. Baumert, L.-H. Chang, A. T. Matsuda, C. J. Tracy, N. G. Cave, R. B. Gregory, and P. L. Fejes, J. Mater. Res. **13**, 197 (1998).
[3] L. C. Sengupta and S. Sengupta, IEEE Trans. Ultrason. Ferroelectr. Freq. Control **44**, 792 (1997).
[4] J. F. Scott, Ferroelectr. Rev. **1**, 1 (1998).
[5] P. C. Joshi and M. W. Cole, Appl. Phys. Lett. **77**, 289 (2000).
[6] W. Chang, J. S. Horwitz, A. C. Carter, J. M. Pond, S. W. Kirchoefer, C. M. Gilmore, and D. B. Chrisey, Appl. Phys. Lett. **74**, 1033 (1999).
[7] A. K. Tagantsev, V. O. Sherman, K. F. Astafiev, J. Venkatesh, and N. Setter, J. Electroceram. **11**, 5 (2003).
[8] X. H. Zhu, J. M. Zhu, S. H. Zhou, Z. G. Liu, N. B. Ming, S. G. Lu, H. L. W. Chan, and C. L. Choy, J. Electron. Mater. **32**, 1125 (2003).
[9] D. Dimos and C. H. Muller, Annu. Rev. Mater. Sci. **28**, 397 (1998).
[10] M. W. Cole, P. C. Joshi, M. H. Ervin, M. C. Wood, and R. L. Pfeffer, Thin Solid Films **374**, 34 (2000).
[11] R. J. Cava, J. Mater. Chem. **11**, 54 (2001).
[12] M. W. Cole, P. C. Joshi, and M. H. Ervin, J. Appl. Phys. **89**, 6336 (2001).
[13] C. L. Chen, J. Shen, S. Y. Chen, G. P. Luo, C. W. Chu, F. A. Miranda, F. W. Van Keuls, J. C. Jiang, E. I. Meletis, and H. Y. Chang, Appl. Phys. Lett. **78**, 652 (2001).
[14] C. L. Canedy, H. Li, S. P. Alpay, L. Salamanca-Riba, A. L. Roytburd, and R. Ramesh, Appl. Phys. Lett. **77**, 1695 (2000).
[15] M. W. Cole, W. D. Nothwang, C. Hubbard, E. Ngo, and M. Ervin, J. Appl. Phys. **93**, 9218 (2003).
[16] D. M. Bubb, J. S. Horwitz, S. B. Qadri, S. W. Kirchoefer, C. Hubert, and J. Levy, Appl. Phys. A: Mater. Sci. Process. **79**, 99 (2004).
[17] O. Auciello, S. Saha, D. Y. Kaufman, S. K. Streiffer, W. Fan, B. Kabius, J. Im, and P. Baumann, J. Electroceram. **12**, 119 (2004).
[18] O. G. Vendik, S. P. Zubko, S. F. Karmanenko, M. A. Nikol'ski, N. N. Isakov, I. T. Serenkov, and V. I. Sakharov, J. Appl. Phys. **91**, 331 (2002).
[19] G. A. Smolensky, in *Ferroelectrics and Related Materials* (Gordon and Breach, New York, 1985).
[20] R. Slowak, S. Hoffmann, R. Liedtke, and R. Waser, Integr. Ferroelectr. **24**, 169 (1999).
[21] X. H. Zhu, H. L. W. Chan, C. L. Choy, and K. H. Wong, J. Vac. Sci. Technol. A **20**, 1796 (2002).
[22] X. H. Zhu, N. Chong, H. L. W. Chan, C. L. Choy, Z. G. Liu, and N. B. Ming, Appl. Phys. Lett. **80**, 3376 (2002).
[23] X. H. Zhu, S. G. Lu, H. L. W. Chan, C. L. Choy, and K. H. Wong, Appl. Phys. A: Mater. Sci. Process. **77**, 225 (2003).
[24] S. G. Lu, X. H. Zhu, C. L. Mak, K. H. Wong, H. L. W. Chan, and C. L. Choy, Appl. Phys. Lett. **82**, 2877 (2003).
[25] S. J. Lee, S. E. Moon, H. C. Ryu, M. H. Kwak, Y. T. Kim, and S. K. Han, Appl. Phys. Lett. **82**, 2133 (2003).
[26] S. J. Lee, S. E. Moon, M. H. Kwak, H. C. Ryu, Y. T. Kim, and S. K. Han, Integr. Ferroelectr. **49**, 151 (2002).